Structure and Dynamics in DNA Looped Domains: CAG Triplet Repeat Sequence Dynamics Probed by 2-Aminopurine Fluorescence†

Benjamin J. Lee,‡ Maryan Barch,‡,§ Edward W. Castner, Jr.,*,‡ Jens Völker,*,‡ and Kenneth J. Breslauer*,‖

Department of Chemistry and Chemical Biology, Rutgers—The State University of New Jersey, 610 Taylor Road, Piscataway, New Jersey 08854, and The Cancer Institute of New Jersey, New Brunswick, New Jersey 08901

Received March 23, 2007; Revised Manuscript Received July 9, 2007

ABSTRACT: The triplet repeat sequence $(CAG)_n$ and related triplet repeats are associated with dynamic DNA mutations implicated in a number of debilitating human diseases. To gain insight into the dynamics of the $(CAG)_n$ repeat, we have substituted a single 2-aminopurine (2AP) fluorescent base for adenine at select positions within the 18 base looped domain of a $(GC)_3(CAG)_6(GC)_3$ hairpin oligonucleotide. Using temperature-dependent steady-state fluorescence measurements in combination with time correlated photon counting spectroscopy, we show the conformation and dynamics of the C**2AP**G domains to be strongly dependent on the position of the probe in the looped region. In other words, rather than being a uniform, single stranded loop, the $(CAG)_6$ triplet repeat looped domain exhibits order and dynamics that are position dependent. The 2AP fluorescence dynamics within the C**2AP**G repeat are well described by a 4 component exponential decay model, with lifetimes ranging from 5 ps to 4 ns. Differences in global DNA conformation (duplex, hairpin, single strand), as well as the local position of the probe within the loop of a given hairpin, predominantly are reflected in the relative amplitude rather than the lifetime of the probe. The time dependent 2AP anisotropy in the hairpin $(CAG)_n$ loops is sensitive to the position of the fluorescent base, with the fluorescence depolarization of a centrally located 2AP probe within the loop proceeding significantly more slowly than 2AP positioned at the 5′- or 3′-end of the repeat sequence near the loop−stem junction. These results are consistent with segmental motions of the CAG repeat, while also suggesting that the 2AP probe is significantly stacked, possibly even hydrogen bonded, within the partially structured CAG looped domain. Our results characterize the position-dependent and conformation-dependent dynamics and order within $(CAG)_n$ triplet repeat DNAs, properties of relevance to the biological mechanisms by which such domains can lead to disease states.

A number of debilitating human diseases with non-Mendelian inheritance patterns have been traced to the uncontrolled expansion of CNG triplet repeat DNA sequences beyond a critical threshold value, where N represents either A, T, G, or C. Huntington's disease, spinobulbar muscular dystrophy (Kennedy disease), Machado−Joseph disease, Haw River syndrome, and a variety of other ataxias and related diseases result from the expansion of $(CAG)_n$ triplet repeats, which is one of the more common triplet repeat sequences associated with DNA expansion diseases (*1*−*6*). Common to these diseases is the uncontrolled expansion of specific repeat sequences from one generation to the next, although the different diseases manifest themselves by different phenotypes and show different clinical symptoms, and the actual disease can be traced to different molecular events following DNA expansion. DNA expansion and subsequent development of disease appears to be preordained once a critical threshold number of triplet repeats (commonly about 30 repeats) has been surpassed. Although the processes that lead to DNA expansion are as yet not fully understood, most experimental evidence points to a malfunction of normal processes of DNA metabolism in repeat sequence domains that lead to DNA expansion during either replication, transcription, or repair (*7*−*10*). A growing body of experimental evidence also suggests that the intrinsic structure and dynamics of the repeat sequences themselves is at least partially responsible for the malfunction of these DNA processes. For this reason, understanding the structural preferences of CNG repeat DNAs, their conformational dynamics, and their thermodynamic properties is of considerable interest.

We recently have described an oligonucleotide based model system in which a triplet repeat $((CNG)_n)$ sequence domain is placed in-between two $(GC)_3$ domains to force formation of a hairpin stem−loop system (*11*) with a triplet repeat loop and a conventional 6-mer Watson and Crick duplex stem. This model system allowed us, for the first time, to determine thermodynamic parameters for single stranded and double stranded triplet repeat sequences without interferences from the considerable conformational heterogeneity typical for highly repetitive DNA fragments (*12*−*25*). Our

† This work was supported by National Institutes of Health Grants GM23509, GM34469 and CA47995 (to K.J.B.), the National Science Foundation Grant NSF-CHE-0239390 (to E.W.C.), and the Donors of the ACS Petroleum Research Fund (to E.W.C.).

* To whom correspondence should be addressed. E-mail: jvolker@rci.rutgers.edu, kjbdna@rci.rutgers.edu, ed.castner@rutgers.edu.

‡ Rutgers—The State University of New Jersey.

§ Present address: Department of Chemistry, Massachusetts Institute of Technology, 77 Massachusetts Avenue, Cambridge, MA 02139-4307.

‖ The Cancer Institute of New Jersey.

10.1021/bi7005674 CCC: $37.00
Published on Web 08/25/2007

Scheme 1: Substitution of 2-Aminopurine (2AP) at Selective Positions in the Parent Hairpin Sequence d[$(GC)_3(CAG)_6(GC)_3$], Along with the Abbreviated Nomenclature for Each Hairpin

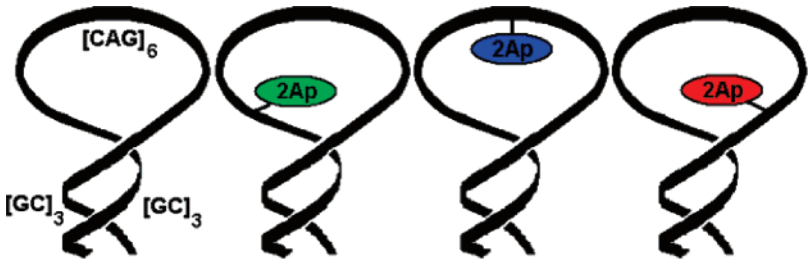

experimental results suggest that single stranded $(CAG)_n$ and $(CTG)_n$ triplet repeat sequences within the hairpin molecule adopt an ordered state or family of closely related microstates that contribute significantly to the overall thermodynamics of the hairpin molecules. Such order may well contribute to the processes that lead to DNA expansion, and ultimately to the diseased state (*26*). Thermodynamic studies alone are unable to explore the conformational and dynamic features of the repeat sequences that cause the measured increase in thermodynamic order. In an effort to gain additional insight into the structural and dynamic features of the $(CAG)_n$ repeat sequence, we report here on the properties of the $(CAG)_6$ triplet repeat hairpin in which we have selectively replaced a single adenine by its fluorescent analogue 2-aminopurine (2AP).

2-Aminopurine is a fluorescent analogue of adenine that has been shown to only minimally perturb DNA structure and stability (*27*, *28*). Like adenine, 2AP base pairs with thymine in a Watson−Crick geometry, but it can also base pair with cytosine, and is highly mutagenic when incorporated in DNA (*27*−*31*). 2AP can be selectively excited at wavelengths between 300 and 330 nm, where conventional DNA bases do not absorb. The peak of the 2AP fluorescence in aqueous solutions is at 371 nm, and it displays a single decay time constant of about 10.4 ns for the free base. When incorporated into DNA, 2AP fluorescence is extensively quenched in a sequence and conformation dependent manner (*32*−*38*). 2AP in DNA exhibits multiexponential transients that generally have substantially shorter lifetimes than that of the free base. Because of its spectroscopic and fluorescent properties, 2AP has been used frequently to probe structural, dynamic, solvation, hydration, and electron transfer/hole transfer aspects of DNA and RNA structures and their interactions with ligands and proteins (*39*−*54*). These properties also make 2AP a convenient probe for investigating triplet repeat sequences.

Our goal here is to make use of 2AP to gain insight into the local structure and dynamics of CAG repeats using steady-state fluorescence, fluorescence lifetime, and fluorescence anisotropy measurements. To this end, we synthesized three $(GC)_3(CAG)_6(GC)_3$ hairpin molecules in which we selectively replaced a single adenine with 2AP at three positions: namely, the adenine in the first CAG repeat to form the $(GC)_3${5′-2AP-d$[CAG]_6$}$(GC)_3$ hairpin [abbreviated as 5′-2AP-d$[CAG]_6$]; an adenine at the third CAG repeat near the middle of the sequence to form the $(GC)_3${mid-2AP-d$[CAG]_6$}$(GC)_3$ hairpin [abbreviated as mid-2AP-d$[CAG]_6$], and the adenine in the sixth (last) CAG repeat to form the $(GC)_3${3′-2AP-d$[CAG]_6$}$(GC)_3$ hairpin [abbreviated as 3′-2AP-d$[CAG]_6$] (Scheme 1). Henceforth, we will refer to the three AP-substituted 30-mer hairpins as either the 5′-2AP-$[CAG]_6$, the mid-2AP-d$[CAG]_6$, or the 3′-2AP-d$[CAG]_6$ hairpin sequence, with the terminal GC stem duplex domains implied but not shown for each designation.

We show below that incorporation of a single 2AP in place of adenine only minimally perturbs the global properties of the repeat sequence as measured by UV spectroscopy and calorimetry. However, CD spectroscopy and steady-state fluorescence measurements reveal differences in the spectral properties of the three model hairpin molecules that suggest position dependent differences in local structure and dynamics. Isotropic and anisotropic fluorescent lifetime measurements allow insight into the origins of the position dependence of the 2AP fluorescence and reveal dynamic processes specific to the $(CAG)_n$ loop. Our results suggest not only that 2AP in the $(CAG)_n$ repeat loop differs significantly from 2AP in single strands and 2AP in 2AP·T base pair within a duplex but also that 2AP properties depend on the position of the fluorophore within the triplet repeat domain. These results highlight the unusual properties of $(CAG)_n$ repeats that may contribute to the processes that lead to the development of DNA expansion and ultimately to triplet expansion diseases.

MATERIALS AND METHODS

Materials. Oligonucleotides d$[CAG]_6$, 5′-2AP-d$[CAG]_6$, mid-2AP-d$[CAG]_6$, 3′-2AP-d$[CAG]_6$, and the complementary d$[CTG]_6$ were synthesized using an Expedite 8900 DNA synthesizer by conventional phosphoramidite chemistry and purified by repeated DMT-on and DMT-off reverse phase HPLC on a PRP reverse phase HPLC column (Hamilton) as previously described (*11*). 2-Aminopurine phosphoramidite was purchased from Glen Research and used according to manufacturer recommendations. Purified oligonucleotides were dialyzed against at least 2 exchanges of a pH 6.8 buffer containing 10 mM sodium cacodylate and 1 mM EDTA with sufficient NaCl added to give a total concentration of 100 mM in Na^+ ions. Stock concentrations were determined spectrophotometrically using molar extinction coefficients determined by phosphate analysis (*55*, *56*). The molar extinction coefficients for the single stranded state (at 90 °C) were as follows: d$[CTG]_6$ (260 nm, 90 °C) = 280,000 M^{-1} cm^{-1}; d$[CAG]_6$ (260 nm, 90 °C) = 308,000 M^{-1} cm^{-1}; 2AP-d$[CAG]_6$ (260 nm, 90 °C) = 298,500 M^{-1} cm^{-1}. As expected, the molar extinction coefficient for all three

2-aminopurine containing oligonucleotides were within experimental error of each other so only a single extinction coefficient is listed. The reduction in extinction coefficient relative to the parent d[CAG]$_6$ sequence is in line with expectations based on the known extinction coefficients of adenine vs 2-aminopurine.

UV Spectroscopy. UV spectra as a function of temperature were recorded using an Aviv DS 14 UV/vis spectrophotometer equipped with a 5 cell thermoelectric cell holder. Samples ($C_t = 2\mu M$) in semi-micro quartz cuvettes of 10 mm path length were heated in steps of 0.5 °C from 0 to 100 °C, and the absorbance was recorded at 260, 270, 282, and 290 nm. After each temperature was reached, the instrument was allowed to equilibrate for 1 min before recording the absorbance values with an averaging time of 5 s, giving rise to a nominal heating rate of 0.1 °C/min. After subtraction of appropriate buffer blanks the UV melting curves were analyzed as previously described (*57*−*59*).

CD Spectroscopy. CD spectra as a function of temperature were recorded using an Aviv DS 62 spectropolarimeter equipped with thermoelectric cell holder. $C_t = 15\ \mu M$ samples in 0.1 cm or 1 cm path length quartz cuvettes were equilibrated for 1 min at each temperature before measuring the CD spectra between 360 and 200 nm (220 nm) in 1 nm increments with an integration time of 5 s. Spectra were recorded in increments of 5 °C between 0 and 95 °C. Longer cells with 10 mm path were required to resolve the 2AP CD bands between 300 and 340 nm. Appropriate buffer spectra were recorded separately and subtracted from the sample spectra before normalization with respect to concentration as previously described (*60*).

Differential Scanning Calorimetry (DSC). DSC traces were recorded using a Nano II DSC differential scanning calorimeter (Calorimetry Science Corporation, Provo, UT). Dialyzed oligonucleotides at nominal concentrations of 50 μM were repeatedly scanned from 0 to 100 °C at a constant heating rate of 1 °C per minute, and the excess power required to maintain identical temperature in sample and reference cells was recorded. After correction for heating rate and subtraction of the appropriate buffer vs buffer curves, the apparent heat capacity curves were normalized with respect to oligonucleotide concentrations and analyzed as described (*59*). ΔH_{cal} values were derived by integration of the area enclosed by the excess heat capacity curve and the extrapolated baselines. ΔS_{cal} values were derived by integration of the C_p/T curves, and ΔC_p was estimated from the difference in the linearly extrapolated pre- and post-transition baselines at T_m. The T_m corresponds to the maximum of the excess heat capacity curve.

Steady-State Fluorescence Spectroscopy. Steady-state fluorescence emission and excitation spectra were recorded using a Varian Eclipse fluorimeter equipped with 4 cell thermoelectric cell holder or a Spex Fluoromax-3 photon counting fluorimeter with a thermoelectric temperature-controlled cell holder and quartz polarizers for emission anisotropy experiments. Excitation spectra between 250 and 330 nm and emission spectra between 320 and 520 nm were recorded in steps of 1 nm with a constant bandwidth of 5 nm, averaging time of 1 s, and the most sensitive photomultiplier setting on the Varian instrument, and with 1.5 nm bandwidth, 1 nm/step, 1 s integration time settings on the Spex instrument. Temperature dependent changes in fluorescence were recorded by heating the sample at a rate of 0.2 °C per minute with continuous stirring while exciting at 310 nm and monitoring emissions at 370 nm. Sample concentrations ranged from 2 to 4 μM giving an absorbance value of less than 0.1 at the excitation wavelength.

Time-Correlated Single-Photon Counting. Time-correlated single-photon counting (TCSPC) experiments were performed using a custom built instrument previously described in detail (*61*, *62*). UV excitation light was obtained by frequency tripling the 900 nm fundamental output from the Spectra-Physics Tsunami femtosecond Ti:sapphire laser using a Uniwave Technology TP-1B frequency tripler. A Becker and Hickl model SPC-630 TCSPC data acquisition instrument was used for data collection. To remove polarization bias from the spectrometer grating, an Optics for Research quartz depolarizer was placed in front of the entrance slit of the spectrometer, and vertical polarization was defined by a Glan-Laser polarizer. A matched Glan-Laser polarizer was used as analyzer to detect fluorescence emission at vertical, magic angle (54.7° from the vertical), and horizontal polarization. A 10 mm sample path length was used for each sample.

2AP fluorescence emission decays were obtained from 300 nm excitation and 371 nm emission. Emission decays were read to 10^4 fluorescence counts in a time window of 12.5 ns over 4096 time channels giving a resolution of 3.05 ps/channel. Oligonucleotide concentrations were either 4 μM for fluorescence lifetime measurements or 12 μM for fluorescence anisotropy experiments. These concentrations give rise to an absorbance value of less than 0.1 at 300 nm. Instrument response functions were obtained using 300 nm light using nondairy creamer scattering solutions matching the absorption of each of our samples. Typical response functions had a full width half-maximum value between 27 and 30 ps.

TCSPC Data Analysis. The TCSPC transients were fit to multiexponential decay models using a convolute-and-compare nonlinear least-squares fit algorithm using macros written in IGOR Pro 4.09A. The instrument response function was convoluted with a fit function of 4 exponential terms to fit the isotropic emission decay data by a forward fast Fourier-transform (FFT) method using the IGOR Pro Fit All At Once procedure. The specific model functions used for the vertically polarized excitation, magic-angle polarized emission fluorescence transient data were

$$K(t) = \sum_{i=1}^{4} a_i \exp(-k_i t) \tag{1}$$

where

$$\tau_i = \frac{1}{k_i}$$

Fluorescence polarization anisotropy decays were analyzed by simultaneously fitting the emission transients measured at vertical, magic angle, and horizontal polarizations, generalizing the procedure described by Cross and Fleming in 1984 (*63*). Specifically, the vertical and horizontal emission decays were fit using the functions $I_{VV} = K(t)[1 + 2r(t)]$, $I_{VH} = K(t)[1 - r(t)]$, and $I_{VM} = K(t)$, where $K(t)$ is the isotropic emission decay model described in eq 1 and $r(t)$ is

Table 1: Comparison of Thermodynamic Data

sample	T_m [°C]	ΔH_{cal} [kcal mol^{-1}]	ΔS_{cal} [cal mol^{-1} K^{-1}]	ΔC_p [cal mol^{-1} K^{-1}]
A: For Hairpin ⇔ Coil Transitions				
d[CTG]$_6$	81.5 ± 0.2	109.7 ± 5.4	309.3 ± 15.5	850 ± 127
d[CAG]$_6$	80.9 ± 0.2	86.6 ± 4.3	244.7 ± 12.2	1019 ± 152
5′-2AP-d[CAG]$_6$	82.9 ± 0.2	87.8 ± 4.4	246.7 ± 12.3	889 ± 133
mid-2AP-d[CAG]$_6$	84.2 ± 0.2	88.1 ± 4.4	246.8 ± 12.3	1027 ± 154
3′-2AP-d[CAG]$_6$	82.8 ± 0.2	87.2 ± 4.3	246.0 ± 12.3	1147 ± 172
B: For Duplex ⇔ Coil Transitions				
d[CAG]$_6$·d[CTG]$_6$	89.3 ± 0.2	281.7 ± 14.1	777.1 ± 38.8	1162 ± 174
5′-2AP-d[CAG]$_6$·d[CTG]$_6$	88.9 ± 0.2	274.1 ± 13.7	757.2 ± 37.9	1622 ± 243
mid-2AP-d[CAG]$_6$·d[CTG]$_6$	88.6 ± 0.2	266.4 ± 13.3	736.3 ± 36.8	1022 ± 153
3′-2AP-d[CAG]$_6$·d[CTG]$_6$	88.9 ± 0.2	277.8 ± 13.9	767.3 ± 38.3	1816 ± 272

the fluorescence depolarization law. All three polarization decays were fit simultaneously using a global fit function that fits to a universal set of parameters,

$$r(t) = r_1 \exp\left(\frac{-t}{\theta_{rot,1}}\right) + r_2 \exp\left(\frac{-t}{\theta_{rot,2}}\right) \quad (2)$$

where the $\theta_{rot,I}$ are the time constants for 2AP reorientation, and the sum of r_1 and r_2 is less than 0.4.

RESULTS AND DISCUSSION

The Adenine to 2-Aminopurine Substitution Is Nearly Conformationally and Energetically Neutral. Proper use of the fluorescent 2-aminopurine (2AP) adenine analogue as a probe of local dynamics within CAG repeat sequences requires that the modified base does not significantly alter the sequence-directed intrinsic global and local properties of the CAG repeat. To assess the impact of selectively replacing specific adenines by 2AP in the d[CAG]$_6$ sequence, we thermodynamically characterized the three 2AP-containing hairpin oligonucleotides and their complexes relative to the unmodified parent d[(GC)$_3$(CAG)$_6$(GC)$_3$] sequence. Table 1 lists the results of our UV and DSC melting studies for the three 2AP substituted oligomers. Each of the three d[(GC)$_3${2AP-d(CAG)$_6$}(GC)$_3$] sequences undergoes a single concentration independent melting transition at high temperature, characteristic of a hairpin to coil transition, and each combines with the complementary d[(GC)$_3$(CTG)$_6$-(GC)$_3$] hairpin only at elevated temperature to yield the 30-mer duplex. Once formed, the 30-mer duplex persists, and the hairpin cannot re-form. These results are consistent with those we previously have reported for the unmodified d[(GC)$_3$(CAG)$_6$(GC)$_3$] parent oligonucleotide, revealing that the 2AP substitution does not alter these global properties (*11*).

We previously have shown the CAG$_6$ loop to make a significant contribution in terms of ΔT_m, ΔH, and ΔS to the overall thermodynamic stability of the d[(GC)$_3$(CAG)$_6$(GC)$_3$] hairpin and CAG-Ω-DNA (*11*, *26*). Inspection of the data listed in Table 1 reveals that replacing adenine by 2AP in the CAG$_6$ hairpin loop results in modestly higher T_m values than was measured for the unmodified d[(GC)$_3$(CAG)$_6$(GC)$_3$] parent sequence. This modest increase in T_m is most pronounced for the hairpin sequence with the 2AP substitution toward the middle of the d[CAG]$_6$ looped domain. The thermodynamic origins of these small differences in T_m cannot be defined because the entropy and the enthalpy values are identical to those of the unmodified parent within the margin of error (further evidence of the relatively unperturbing nature of the AP substitution). Significantly, however, other studies consistently report a decrease in T_m when 2AP replaces adenines in DNA and RNA hairpin loops (*46*, *50*, *64*−*67*). Consequently, our observed small increase in T_m for this replacement likely reflects properties specific to the CAG loop domain. By contrast to this A to 2AP induced melting temperature behavior for the hairpin structures, UV and DSC melting curves of all three corresponding 2AP-d[CAG]$_6$·d[CTG]$_6$ duplexes show small *decreases* in T_m (0.4 to 0.7 °C). Thermodynamically, this T_m decrease is due to a decrease in enthalpy (average $\Delta\Delta H_{cal} = -8.9$ kcal/mol) which is partially compensated by an entropy decrease (average $\Delta\Delta S = -23.5$ cal/mol/K) relative to the d[CAG]$_6$·d[CTG]$_6$ parent duplex. These latter results are consistent with previously published data for adenine to 2AP substitutions in DNA duplexes, which contrast with the impact of this substitution on the looped triplet repeat domains on the hairpin structures studies here (*28*). These differences in the thermodynamic consequences of the A to 2AP substitution on the stability of the hairpin and duplex highlight the importance of determining complete thermodynamic profiles for understanding the impact of even conservative base modifications on DNA stability.

In the aggregate, our results suggest that replacing a single adenine by 2AP does not significantly alter the global thermodynamic properties of the CAG triplet repeat hairpin sequences, making 2AP a reasonable probe for the dynamics of CAG$_n$ repeats.

CD Spectroscopy Reveals Subtle Position Dependent Differences in 2AP Environment in the Hairpin State. The CD spectra for the 2AP-substituted d[CAG]$_6$ hairpins shown in Figure 1 are largely similar to the corresponding spectra previously described for the unsubstituted d[(GC)$_3$(CAG)$_6$-(GC)$_3$] hairpin, with subtle differences due to differences in spectral properties of 2AP relative to adenine. Most notable in these spectra is the small CD signal in the 300−340 nm range, which is observed only in the 2AP-containing sequences. This signal recently has been shown by von Hippel and co-workers to be sensitive to the conformational state of 2AP in DNA (*68*). In this work, we also find this 2AP CD band to be sensitive to DNA conformation, with a more pronounced signal for the hairpin than for the duplex state. This CD band is largely absent at elevated temperature when the oligonucleotides are fully denatured. A similar CD band is not seen when 2AP is placed in the center of a control 18 base adenine hairpin loop (data not shown). More importantly, the 300−340 nm CD band is significantly more

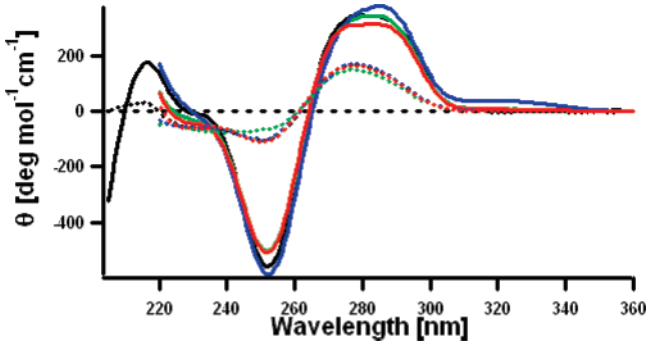

FIGURE 1: CD spectra of unmodified parent hairpin d[CAG]$_6$ (black), 5′-2AP-d[CAG]$_6$ (green), mid-2AP-d[CAG]$_6$ (blue), and 3′-2Ap-d[CAG]$_6$ (red) at 0 °C (solid lines) and 95 °C (dashed lines).

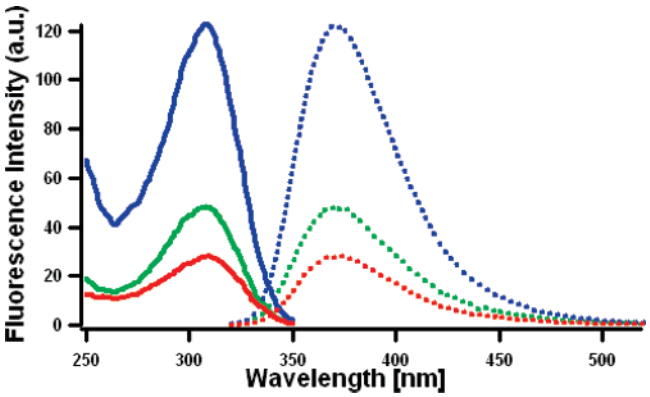

FIGURE 2: Excitation and emission spectra of the 5′-2AP-d[CAG]$_6$ (green), mid-2AP-d[CAG]$_6$ (blue), and 3′-2AP-d[CAG]$_6$ (red) hairpins at 20 °C.

pronounced for the mid-2AP-d[CAG]$_6$ hairpin than for either the 5′-2AP-d[CAG]$_6$ or 3′-2AP-d[CAG]$_6$ hairpins, despite virtually identical UV spectra for all three sequences. By contrast, differences in the measured CD signal with position of the 2AP base within the *duplex* state fall within experimental error (results not shown). The overall similarities of the CD spectra with that of the d[CAG]$_6$ parent hairpin suggest that the three 2AP-containing oligonucleotides adopt the same overall native hairpin conformation, whereas the subtle differences in the CD spectra between the three 2AP-containing hairpins mirror the differences in the T_m we described above. These small differences suggest position dependent differences in the environment or conformation of the 2AP base within identical sequence environments and the same global conformation. As elaborated on below, we use steady-state and time-resolved fluorescence experiments to characterize these position dependent effects.

The Degree of Steady-State Fluorescence Quenching of 2AP Depends on the Position of the Probe in the Repeat Domain. Figure 2 shows the steady-state emission and excitation spectra recorded for the three 2AP substituted hairpins at 20 °C. The emission and excitation maxima for all three hairpins are similar to one another and to that of free 2AP, with the major difference between the three hairpins being the degree of quenching. The absence of a defined shoulder at 260−270 nm in the excitation spectrum of all three hairpins suggests that excitation energy transfer from neighboring adenines to 2AP does not contribute to the overall spectral dynamics of these molecules (*36*, *37*, *43*, *69*, *70*). Although the 2AP base resides in the same sequence environment in all three hairpins, the fluorescence

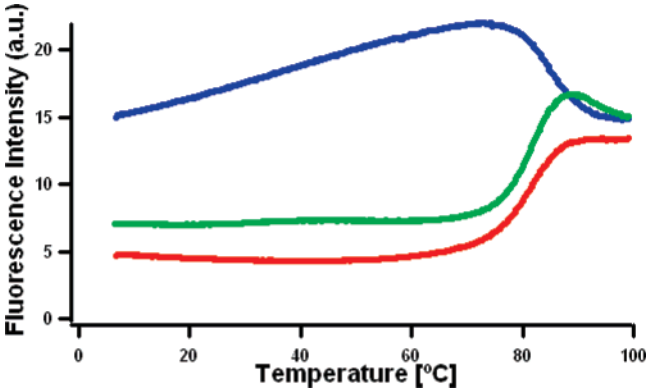

FIGURE 3: Temperature dependence of fluorescence at 370 nm with excitation at 310 nm for the modified hairpins 5′-2AP-d[CAG]$_6$ (green), mid-2AP-d[CAG]$_6$ (blue), and 3′-2AP-d[CAG]$_6$ (red).

of the mid-2AP-d[CAG]$_6$ hairpin is significantly less quenched than either the 5′-2AP-d[CAG]$_6$ or 3′-2AP-d[CAG]$_6$ hairpin. This position dependent behavior suggests differences in local environment, conformation, and dynamics of the fluorophore. These changes in fluorescence properties correlate with similar position dependent differences in the 2AP CD-band, and in T_m, as described above. By comparison, the fluorescence intensity in the duplex state is quenched even more rapidly than in the hairpin state, but the degree of quenching does not depend on the position of the probe (data not shown).

Fluorescence Detected Melting Curves Reveal an Unusual Premelting Transition in the Mid-2AP-d[CAG]$_6$ Hairpin That Is Absent in the 5′- and 3′-2AP Hairpins. Figure 3 shows the temperature dependent changes in steady-state fluorescence intensity at 370 nm (fluorescence detected melting curves) for the three hairpins. The close agreement in T_m determined by UV absorption, calorimetry (DSC), and fluorescence detection suggests that local melting in the vicinity of the probe and global denaturation of the entire molecule occur as a concerted, cooperative process. The position dependent subtle variations in properties for the adenine to 2AP substitution detected by our spectroscopic and thermodynamic measurements do not alter the overall cooperative denaturation of the hairpin molecules. Nevertheless, differences in the shape of the fluorescence detected melting curves highlight position dependent local differences in the 2AP probe that are not detected by other means. In particular, the unusual gradual increase in fluorescence intensity prior to the onset of melting in the mid-2AP-d[CAG]$_6$ sequence is not detected by any other experimental observable, and results in an inverted shape of the melting curve for the mid-2AP-d[CAG]$_6$ hairpin. This observation suggests temperature dependent changes in local dynamics of the mid-2AP base that are absent in the 5′-2AP-[CAG]$_6$ and 3′-2AP-d[CAG]$_6$ hairpins and that are not correlated with global structural changes. By contrast, the fluorescent detected melting curves for the 5′-2AP-[CAG]$_6$ and 3′-2AP-d[CAG]$_6$ hairpins more closely resemble those of the corresponding 30-mer 2AP-d[CAG]$_6$·d[CTG]$_6$ duplexes (not shown), and are similar to those previously reported for other 2AP-containing duplexes (*28*, *37*, *69*). While an increase in the dynamics of a fluorescent probe near the center of a hairpin loop, as in the mid-2AP-d[CAG]$_6$ sequence, is not unexpected, the increase in fluorescence intensity to values significantly larger than those of the high-temperature

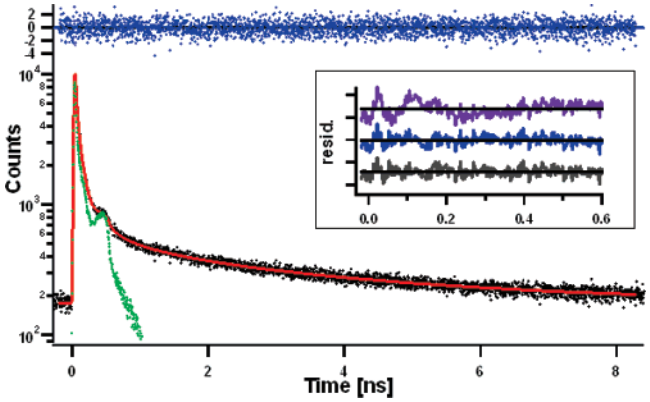

FIGURE 4: Magic angle decay (black) and instrument response function (green) for 3′-2AP-d[CAG]$_6$ at 25 °C fit to four exponential decay functions, along with the corresponding residuals for short times (inset): 3-exponential (purple), 4-exponential (blue), and 5-exponential (gray) fits. The experimental curve and precision of the fit shown are typical for the decay curves measured for 2AP fluorescence in all 3 hairpins.

denatured state suggests that the states sampled by the mid-2AP base differ significantly from those populated in the denatured state. Control experiments (results not shown) with 2AP placed in the center of an all-adenine 18 base hairpin loop show only a gradual decay of fluorescence with temperature, characteristic of temperature induced quenching of solvent accessible fluorophores. Although likely to be partially stacked at low temperature, the adenines in the all adenine hairpin loop are not base paired and melting of the all adenine hairpin cannot be detected by observing the 2AP fluorescence as a function of temperature. This control highlights the unusual temperature dependence of 2AP fluorescence within the hairpin loop CAG repeats. Below, we use isotropic and anisotropic fluorescence lifetime measurements to garner further insight into the position dependent dynamics of the 2AP bases in the context of the steady state measurements just described.

The Isotropic Fluorescence Transients for 2AP in the DNA Structures Are Best Fit to 4-Exponential Models. Figure 4 shows a typical isotropic fluorescence decay transient measured for the mid-2AP-d[CAG]$_6$ hairpin. The solid curve shows the best fit 4-exponential model. Similar transients to the one shown were measured for each of the 2AP-substituted hairpins and duplexes, over a temperature range from 5 to 94 °C. The 4-exponential fit parameters for the three 2AP-d[CAG]$_6$ hairpins and the duplexes at 5 °C are listed Table 2. Fit parameters for the other temperatures are given in the Supporting Information. The 4-exponential lifetime model is consistent with previously published reports (*32*, *44*, *46*, *49*, *52*), although there is some evidence in our data for a sub-picosecond fifth lifetime component that is well below our time resolution (*41*, *42*). Like these prior authors we find that attempts to fit our data with other commonly employed models for fluorescence decay such as stretched exponentials were not successful. Nevertheless, some caution must be exercised in attributing the observed lifetimes to discrete conformations. Our convolute-and-compare nonlinear least-squares fitting routines are unable to resolve more than 4- or 5-exponential components from simulated data created with a broad distribution of up to 12 relaxation components ranging from 1 ps to 5 ns. Thus, our data quality and analysis methods, while competitive with the best available TCSPC data, cannot preclude the possibility of a distribution containing more than four exponential components. Nevertheless, the 4-exponential fit model provides the simplest representation of the conformational dynamics of 2AP in our hairpin models, and is consistent with previously published work.

Position Dependent Variation in 2AP Fluorescence Intensity Is a Consequence of Variations in Amplitude Rather Than Decay Time Constant. Inspection of Table 2 reveals that exponential decay time constants for the 2AP emission from the three hairpins fall into 4 distinct, well-resolved time domains of about 15 ps, 70 ps, 500 ps, and 4 ns. The corresponding decay constant for the three 2AP-d[CAG]$_6$·d[CTG]$_6$ duplexes of 5 ps, 70 ps, 500 ps, and 4 ns differ only in the fastest lifetime (5 ps vs 15 ps) compared with those for the hairpins. These values are similar to those reported by Van Amerongen et al. (*46*) for an isolated base paired C**2AP**G·CTG sequence within a complex DNA hairpin stem/bulge loop structure, and differ somewhat from reported 2AP lifetimes in a different sequence context (*44*, *48*, *49*). Aside from the fastest time constant τ_1, all other time constants primarily reflect the influence of the bases flanking the fluorophore, independent of the global conformation and/or position of the 2AP base. Even the longest lifetime we observe of about 4 ns is significantly shorter than the time constant for free 2AP (10.4 ns). There is no evidence for a longer time constant that would suggest contributions to the emission profile either from free 2AP or from incorporated 2AP that is fully exposed to solvent. By contrast, the oligonucleotide conformation and position of the 2AP base within the sequence are reflected in the normalized amplitudes giving rise to the significant differences in integrated (or steady-state) fluorescence. For the duplex, an excess of 90% of the fluorescence transients correspond to the shortest relaxation time constant (τ_1 = 5 ps), whereas in the hairpins the shortest time constant (τ_1 = 15 ps) contributes only about 70% of the fluorescent transients. The increase in steady-state fluorescence of the mid-2AP-d[CAG]$_6$ hairpin relative to the 5′-2AP-d[CAG]$_6$ and 3′-2AP-d[CAG]$_6$ hairpins is a consequence of the increased contribution of the long lifetime decay (τ_4), with a corresponding reduction in normalized amplitude of the shortest lifetime (τ_1). In the aggregate, these data reveal that the position-dependent variation in 2AP fluorescence inten-

Table 2: 2AP Time Constants for Hairpin and Duplex Structures at 5 °C

sequence	a_1	τ_1 [ns]	a_2	τ_2 [ns]	a_3	τ_3 [ns]	a_4	τ_4 [ns]
5′-2AP-d[CAG]$_6$	0.713	0.015	0.256	0.063	0.021	0.362	0.010	4.128
mid-2AP-d[CAG]$_6$	0.600	0.017	0.166	0.086	0.163	0.562	0.071	3.995
3′-2AP-d[CAG]$_6$	0.748	0.017	0.224	0.072	0.020	0.393	0.008	3.680
5′-2AP-d[CAG]$_6$·d[CTG]$_6$	0.988	0.001	0.011	0.083	0.004	0.557	0.004	4.282
mid-2AP-d[CAG]$_6$·d[CTG]$_6$	0.947	0.004	0.027	0.062	0.015	0.516	0.010	3.967
3′-2AP-d[CAG]$_6$·d[CTG]$_6$	0.935	0.006	0.044	0.060	0.012	0.524	0.009	3.803

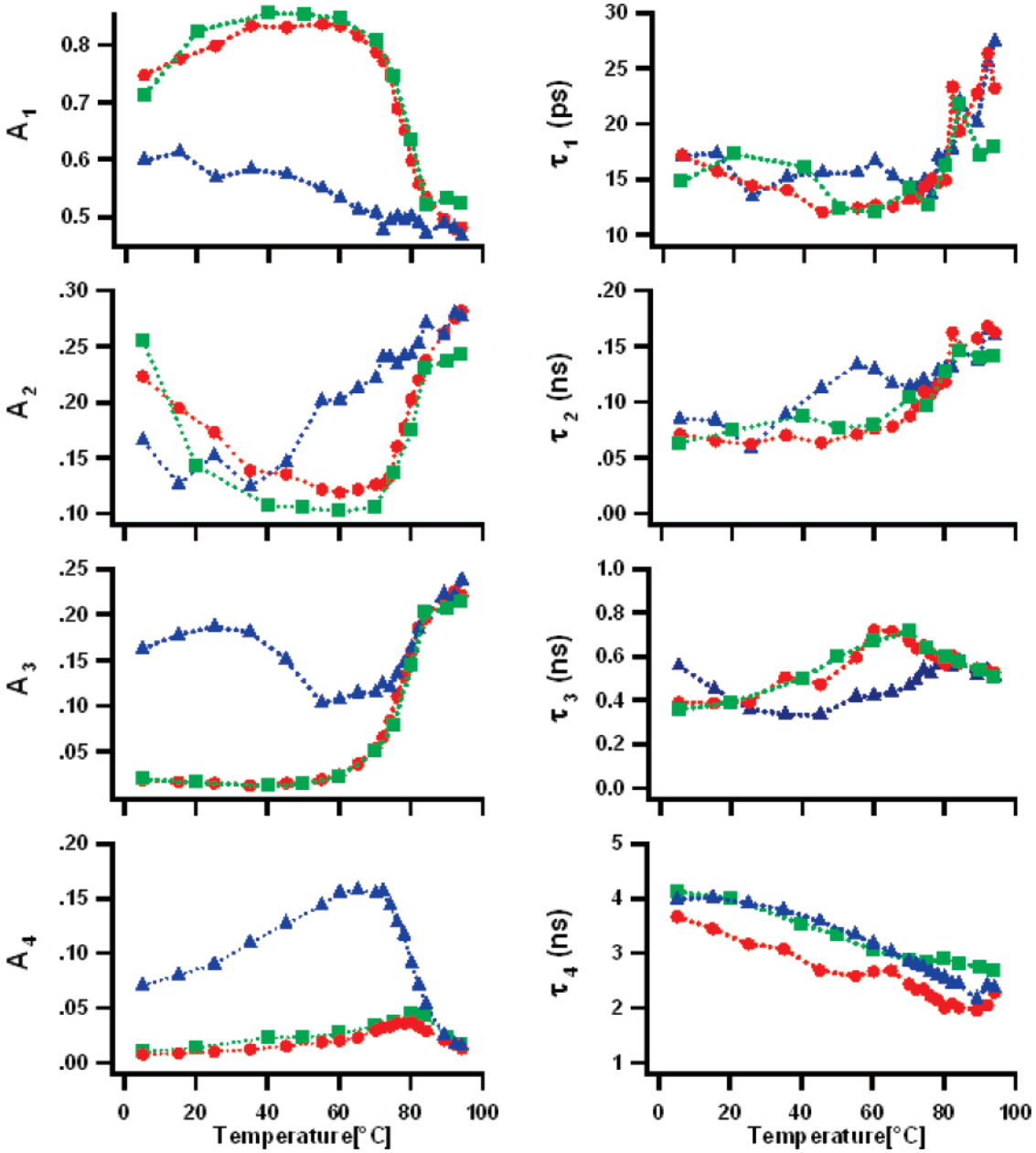

FIGURE 5: Normalized amplitudes and decay lifetimes for the 5′-2AP-d[CAG]$_6$ (green), mid-2AP-d[CAG]$_6$ (blue), and 3′-2AP-d[CAG]$_6$ (red) hairpins from 5 to 94 °C.

sity is reflected in variations in the amplitude rather than in the decay time constant.

The Normalized Amplitude Reflects the Conformational State While the Time Constant Predominantly Reflects the Impact of Neighboring Bases. For each of the three hairpins, Figure 5 shows the temperature dependence of the normalized amplitudes and corresponding time constants obtained for the 4-exponential fits to the 2AP emission transients. The amplitude averaged lifetime plotted against temperature (not shown) for these data shows the same shapes as the steady-state fluorescence melting curves described above, suggesting that all salient features of the emission processes are captured. Characteristically, almost all the normalized amplitudes associated with these lifetimes tend to exhibit the sigmoidal temperature dependence typical of oligonucleotide melting transitions, whereas the time constants, in general, do not show such sigmoidal temperature dependencies. This behavior is consistent with our interpretation that the normalized amplitude reflects the conformational state of the oligonucleotide whereas the time constant predominantly reflects the impact of neighboring bases. Moreover, apparent thermal midpoints (or T_m values) determined from the normalized amplitudes vs temperature curves are similar to those detected by conventional melting techniques, at least within the (limited) temperature resolution of these experiments. This observation suggests that concerted global changes in DNA secondary structure also are reflected in the local processes that give rise to the 4 time constants. Consequently, those instances where the normalized amplitude does not conform to the classical sigmoidal melting curve are of particular interest, and are discussed in more detail below. In general, melting of the DNA secondary structure appears to result predominantly in a redistribution of populations (amplitude) associated with a particular lifetime rather than significant changes in the nature of a particular emitting state (time constant).

Within our DNA construct, only the fastest time constant directly reflects temperature induced disruption of base pairing/stacking. Results by Zewail and co-workers (*41*, *42*, *71*) suggest that this very fast lifetime is at least partially due to rapid hole transfer to neighboring guanines, which should be favored in the more rigidly stacked and base paired duplex state over the more flexible hairpin state, possibly explaining the 3-fold difference in τ_1 between these conformations. Disruption of the conformation allowing hole transfer could explain the increase in lifetime upon denaturation to the coil-like denatured state. In this view, differences in the fastest lifetime predominantly reflect dynamics (gating) of the 2AP conformation.

The Premelting Transition Observed in the Fluorescent Detected Melting Curves of the Mid-2AP-d[CAG]$_6$ Hairpin Is a Consequence of Changes in the Normalized Amplitude of τ_1 and τ_4. In general, the observed increase in total fluorescent intensity upon denaturation of 2AP-containing oligonucleotides (decreased quenching rate) is due to a decrease in normalized amplitudes for τ_1 (inverted shape of melting curve). This observation correlates with an increase in the normalized amplitudes for τ_2 and τ_3 (conventional melting curve shape), with only insignificant changes in the amplitude of τ_4. The exception is the mid-2AP-d[CAG]$_6$ hairpin, where prior to the onset of melting a gradual decrease in the normalized amplitude of τ_1 with temperature is coupled with a corresponding increase in normalized amplitude of τ_4. The onset of melting of the mid-2AP-d[CAG]$_6$ hairpin causes a decrease of the normalized amplitude for τ_4. It is τ_4 that is predominantly responsible for the unusual shape of the fluorescence detected melting curve of the mid-2AP-d[CAG]$_6$ hairpin. Interestingly, the amplitude a_4 increases in the 3′-2AP and 5′-2AP hairpins, as well as for the three duplexes, only in the temperature range where melting occurs, and is noticeably smaller in either the native state at lower temperatures or the denatured state at higher temperatures. These observations suggest that the τ_4 time constant responsible for the unusual fluorescent properties of the mid-2AP-d[CAG]$_6$ hairpin requires increased flexibility and perhaps partial disruption of native structure, but has a small amplitude in the denatured state where base motions are least restricted. Judging by the observed changes in normalized amplitude for τ_4 prior to melting, the increase in 2AP dynamics occurs only when the probe is positioned near the center of the CAG repeat, but not when it is close to the hairpin duplex stem.

Fluorescence Anisotropy Curves Are Best Fit by a 2-Exponential Anisotropy Time Constant Model. Figure 6 shows a typical fluorescence polarization anisotropy decay curve we have measured for the mid-2AP-d[CAG]$_6$ hairpin. Similar results have been obtained for the other hairpins, and for the 3′-2AP-d[CAG]$_6$•d[CTG]$_6$ duplex (not shown). Sample constraints and the low fluorescence quantum yield for 2AP in the duplex state prevent measuring the anisotropy decay for the other two duplexes. However, we do not expect the anisotropy decay for the 5′-2AP-d[CAG]$_6$•d[CTG]$_6$ and mid-2AP-d[CAG]$_6$•d[CTG]$_6$ duplex to differ significantly from that of the 3′-2AP duplex, given that the 2AP probe resides in the same sequence environment within the 30-mer Watson and Crick duplex. We find that the experimental data is best fit to a 2-exponential anisotropy model (*72*−*75*), consistent with similar measurements by others (*32*, *44*, *46*, *76*, *77*). Experimental anisotropy data for 2AP (and other fluorophores) in oligonucleotides frequently can only be fit to a 2-exponential anisotropy model, although the molecular motions giving rise to the observed anisotropy are likely to be more complex and may involve more time domains. Along those lines, we tested and rejected models involving more than 2-exponential time constants and models with 2-exponential anisotropy time constants plus a small $r(\infty)$ term because of insignificant improvements in the fit upon inclusion of the additional parameters, coupled with significant covariance uncertainties (up to ±100%). The fit parameters for the polarization anisotropy transients at 20 and 94 °C are listed in Table 3. Fit parameters at other temperatures are listed in the Supporting Information.

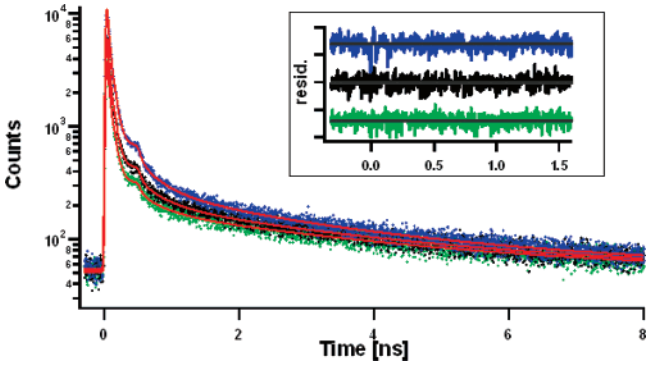

FIGURE 6: Sample polarization anisotropy decay of the 3′-2AP-d[CAG]$_6$ hairpin. The vertical (blue), magic (black), and horizontal (green) emission transients were fit simultaneously with a universal set of parameters for $I_{VV} = I_{VM}[1 + 2r(t)]$ and $I_{VH}[1 - r(t)]$ where $r(t)$ is the anisotropy decay. $r(t)$ is best fit to a double exponential model for all three hairpins.

Table 3: Polarization Anisotropy Results for Hairpin and Duplex Structures at 20 °C

sequence	temp (°C)	r_0	r_1	r_2	θ_{rot1} (ns)	θ_{rot2} (ns)
5′-2AP-d[CAG]$_6$	20	0.326	0.171	0.155	0.328	2.946
mid-2AP-d[CAG]$_6$	20	0.255	0.175	0.079	0.711	3.396
3′-2AP-d[CAG]$_6$	20	0.315	0.170	0.145	0.357	3.086
3′-2AP-d[CAG]$_6$•d[CTG]$_6$	20	0.328	0.182	0.146	0.425	3.685
5′-2AP-d[CAG]$_6$	94	0.291	0.172	0.118	0.047	0.191
mid-2AP-d[CAG]$_6$	94	0.300	0.189	0.111	0.048	0.188
3′-2AP-d[CAG]$_6$	94	0.289	0.200	0.089	0.050	0.228
3′-2AP-d[CAG]$_6$•d[CTG]$_6$	94	0.307	0.263	0.044	0.078	1.490

Components of the Anisotropy r(0) Values. The $r(0)$ values recovered from our deconvolution approach by summing the individual $r_i(0)$ do not add up to the theoretical limiting value of 0.4. Instead they cluster around 0.27−0.34, and are somewhat smaller than those reported for 2AP-containing oligonucleotides by others (*44*, *46*, *77*). This discrepancy may, in part, reflect the non-collinear absorption and emission transition dipoles of 2AP (*78*), as well as ultrafast quenching by solvent and/or energy transfer to neighboring guanines. It is interesting that we find the $r(0)$ values for the native mid-2AP-d[CAG]$_6$ hairpin to be consistently lower (on average $r(0) = 0.27$) than those measured for the 5′-2AP hairpin (average $r(0) = 0.32$), the 3′-2AP hairpin (average $r(0) = 0.32$), the 3′-2AP duplex (average $r(0) = 0.34$), or the $r(0)$ values of all three molecules in the denatured state at 94 °C ($r(0) = 0.30$). These observations suggest that 2AP in the mid-2AP molecules undergoes fast depolarizing motions that we cannot resolve experimentally and that are

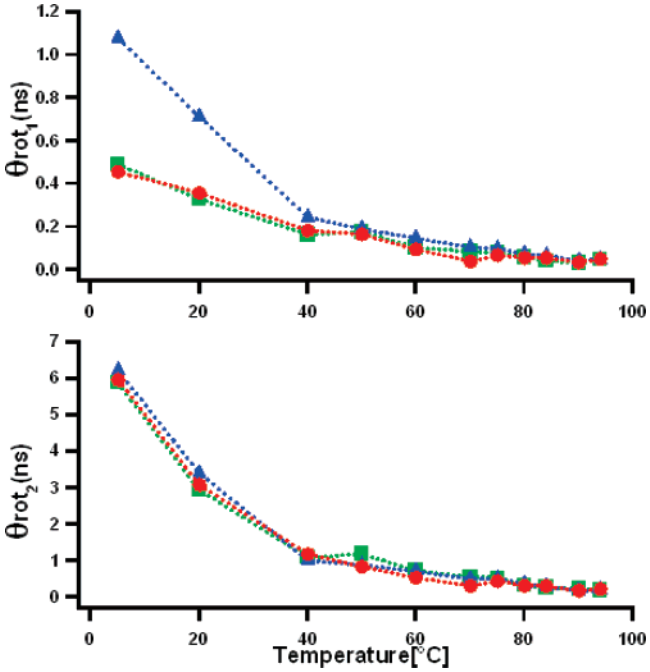

FIGURE 7: Fast (top) and slow (bottom) rotational correlation lifetimes for the 5′-2AP-d[CAG]$_6$ (green), mid-2AP-d[CAG]$_6$ (blue), and 3′-2AP-d[CAG]$_6$ (red) modified hairpins from 5 to 94 °C.

missing in our summation of the $r(0)$ value, an observation that is also supported by our data simulations. Such fast depolarization motions are also missing in the anisotropy time constants discussed below. The degree of the fast depolarization mode depends on the overall conformation of the molecule (duplex < hairpin < single strand), and the position of the probe within the hairpin loop. It is of particular interest that the mid-2AP-hairpin, which shows the highest total fluorescent intensity, also has the lowest $r(0)$ value. The $r(0)$ value for the mid-2AP-hairpin state is even smaller than that measured for the denatured molecule at 94 °C where base motions are least restricted. The contribution of those motions to the overall anisotropy that are too fast to be resolved by the 2-exponential anisotropy model is most pronounced in the mid-2AP-hairpin.

The Slow Anisotropy Time Constant Reflects Motion of the Entire Molecule. Figure 7 shows the temperature dependence of the two anisotropy time constants we have recovered for all three hairpin molecules. Characteristically, the slower rotational anisotropy (which contributes between 50 and 60% of the amplitude of the total anisotropy) is identical for all three hairpins, whereas the fast anisotropy components depend on the position of the probe within the hairpin loop. Using a simplified model which represents the hairpins as stiff rods with B-DNA type parameters (23 Å diameter, 3.4 Å pitch, 15 bp), we identify the slow anisotropy components as reflecting rotation of the entire molecule around its longitudinal (helical) *Z*-axis, with rotation around the *X*-and *Y*-axes being too slow to be detected given the short 2AP lifetimes. This proposed interpretation is consistent with the ethidium bromide fluorescence results of Lu et al. (*79*) who report rotational relaxation time constants in the range of 8−16 ns and 20−90 ns for conventional Watson and Crick duplexes having comparable number of base pairs. For all three hairpins, the slow rotational time constant shows Arrhenius behavior over the entire temperature range, with an activation enthalpy barrier of 7.6 kcal/mol, likely reflecting friction due to interactions with solvent and/or counterions.

The Fast Anisotropy Time Constant Reflects Segmental Motion of the Triplet Repeat Loop Domain. Of particular interest is the fast anisotropy component we have recovered, as this value reflects local motion of the 2AP base. Intriguingly, the fast rotational relaxation times for all three hairpins are significantly slower than that of the 3′-2AP duplex. Moreover, the rotational correlation time is slowest for the mid-2AP hairpin where the 2AP base is near a putative hairpin turn and is least quenched. The fast anisotropy time constant for the mid-2AP hairpin is about 2-fold slower than that of the 5′- and 3′-2AP hairpins at 5 °C, and is too slow to represent motions of a free, non-hydrogen-bonded, unstacked 2AP base. We therefore propose that the fast anisotropy time constant predominantly reflects segmental motions of the hairpin loop (twisting/bending), and/or possibly dynamic changes in base pairing interactions within the triplet repeat loop. Motions of the free unpaired 2AP base likely are responsible for the missing $r_3(0)$ component that cannot be resolved experimentally. The degeneracy of the repeat sequence in the CAG loop domain allows dynamic changes in base pairing interactions with minimal energetic penalty. However such redistributions of base pairing interactions encounter a significant activation barrier and are likely to be slow compared to free base motions. From the temperature dependence of the fast anisotropy, we estimate that the fast motion associated with depolarization of the 2AP base requires an activation energy of between 5 kcal/mol (5′-2AP-d[CAG]$_6$ and 3′-2AP-d[CAG]$_6$) and 7 kcal/mol (mid-2AP-d[CAG]$_6$), confirming that the motions leading to the fast depolarization of 2AP in the CAG hairpin loop are significantly hindered. The activation energy we have measured for the segmental motion is roughly equivalent to the enthalpy required to disrupt one conventional Watson and Crick base pair, or between 3 and 5 base/base interactions in the single strand CAG loop. By comparison, the fast rotational correlation time for the 3′-2AP-d[CAG]$_6$·d[CTG]$_6$ duplex is in line with similar values previously reported for 2AP base paired to thymine in Watson and Crick duplexes, and represents restricted motions possibly between a base paired and an unpaired state of the 2AP base within the confines of the intact double helix. The measured activation energy of between 3 and 4 kcal/mol for the fast depolarization of the 3′-2AP duplex is roughly in line with base pair opening enthalpies for 2AP·T base pairs.

CONCLUSIONS

We have shown that 2-aminopurine is a convenient fluorescent probe for monitoring the dynamics of CAG repeats implicated in triplet expansion diseases. Our results reveal significant differences in the fluorescent properties and dynamics of the 2AP base depending on the type of secondary structure (triplet repeat loop, duplex, or single strand) of the oligonucleotide, as well as the position of the probe within the (CAG)$_n$ repeat. In particular, we find that the steady-state fluorescence, the distribution of lifetimes, and the anisotropy of the 2AP probe near the center of the CAG repeat differ significantly from those of the 2AP probe close to the hairpin stem. Given that the 2AP base is always in the same sequence environment in the models studied here, the observed differences reflect position dependent variations

in conformation and dynamics within the repeat DNA domain. For the hairpin structure, our data are consistent with significant order within the triplet repeat, looped domain. It can be expected that interactions with components of the cellular DNA repair and replication machinery are sensitive to conformational and dynamic processes in the triplet repeat DNA. The *in vitro* conformational and dynamic effects within triplet repeat looped domains defined in this study may have *in vivo* implications for the biological processes that lead to the genotype of DNA expansion and, ultimately, to the phenotype of the diseased state. More generally, our results contribute to the growing literature on the dynamic and thermodynamic properties of unusual, noncanonical DNA structures that may be involved in biological regulatory mechanisms, as well as in the expression of genetic disorders.

ACKNOWLEDGMENT

We thank Dr. G. Eric Plum (IBET Inc/Rutgers University) and Dr. Horst H. Klump (University of Cape Town) for many helpful discussions.

SUPPORTING INFORMATION AVAILABLE

Discussion of data limits, tables with 2AP time constants and anisotropy results at all temperatures. This material is available free of charge via the Internet at http://pubs.acs.org.

REFERENCES

1. Ashley, C. T., Jr., and Warren, S. T. (1995) Trinucleotide repeat expansion and human disease, *Annu. Rev. Genet.* 29, 703−728.
2. Mitas, M. (1997) Trinucleotide repeats associated with human disease, *Nucleic Acids Res. 25*, 2245−2254.
3. Cummings, C. J., and Zoghbi, H. Y. (2000) Trinucleotide repeats: mechanisms and pathophysiology, *Annu. Rev. Genomics Hum. Genet. 1*, 281−328.
4. Sinden, R. R., Potaman, V. N., Oussatcheva, E. A., Pearson, C. E., Lyubchenko, Y. L., and Shlyakhtenko, L. S. (2002) Triplet repeat DNA structures and human genetic disease: dynamic mutations from dynamic DNA, *J. Biosci. 27* (Suppl. 1), 53−65.
5. Pearson, C. E., and Sinden, R. R. (1998) Trinucleotide repeat DNA structures: dynamic mutations from dynamic DNA, *Curr. Opin. Struct. Biol. 8*, 321−330.
6. Sinden, R. R. (1999) Biological implications of the DNA structures associated with disease-causing triplet repeats, *Am. J. Hum. Genet. 64*, 346−353.
7. Jakupciak, J. P., and Wells, R. D. (2000) Genetic instabilities of triplet repeat sequences by recombination, *IUBMB Life 50*, 355−359.
8. Bowater, R. P., and Wells, R. D. (2001) The intrinsically unstable life of DNA triplet repeats associated with human hereditary disorders, *Prog. Nucleic Acid Res. Mol. Biol. 66*, 159−202.
9. Bacolla, A., and Wells, R. D. (2004) Non-B DNA conformations, genomic rearrangements, and human disease, *J. Biol. Chem. 279*, 47411−47414.
10. Wells, R. D., Dere, R., Hebert, M. L., Napierala, M., and Son, L. S. (2005) Advances in mechanisms of genetic instability related to hereditary neurological diseases, *Nucleic Acids Res. 33*, 3785−3798.
11. Völker, J., Makube, N., Plum, G. E., Klump, H. H., and Breslauer, K. J. (2002) Conformational energetics of stable and metastable states formed by DNA triplet repeat oligonucleotides: implications for triplet expansion diseases, *Proc. Natl. Acad. Sci. U.S.A. 99*, 14700−14705.
12. Gacy, A. M., Goellner, G., Juranic, N., Macura, S., and McMurray, C. T. (1995) Trinucleotide repeats that expand in human disease form hairpin structures in vitro, *Cell 81*, 533−540.
13. Gacy, A. M., and McMurray, C. T. (1994) Hairpin formation within the human enkephalin enhancer region. 1. Kinetic analysis, *Biochemistry 33*, 11951−11959.
14. Gacy, A. M., and McMurray, C. T. (1998) Influence of hairpins on template reannealing at trinucleotide repeat duplexes: a model for slipped DNA, *Biochemistry 37*, 9426−9434.
15. Mitas, M., Yu, A., Dill, J., and Haworth, I. S. (1995) The trinucleotide repeat sequence $d(CGG)_{15}$ forms a heat-stable hairpin containing G^{syn}•G^{anti} base pairs, *Biochemistry 34*, 12803−12811.
16. Yu, A., Barron, M. D., Romero, R. M., Christy, M., Gold, B., Dai, J., Gray, D. M., Haworth, I. S., and Mitas, M. (1997) At physiological pH, $d(CCG)_{15}$ forms a hairpin containing protonated cytosines and a distorted helix, *Biochemistry 36*, 3687−3699.
17. Chen, X., Mariappan, S. V., Catasti, P., Ratliff, R., Moyzis, R. K., Laayoun, A., Smith, S. S., Bradbury, E. M., and Gupta, G. (1995) Hairpins are formed by the single DNA strands of the fragile X triplet repeats: structure and biological implications, *Proc. Natl. Acad. Sci. U.S.A. 92*, 5199−5203.
18. Chen, X., Mariappan, S. V., Moyzis, R. K., Bradbury, E. M., and Gupta, G. (1998) Hairpin induced slippage and hyper-methylation of the fragile X DNA triplets, *J. Biomol. Struct. Dyn. 15*, 745−756.
19. Mariappan, S. V., Catasti, P., Chen, X., Ratliff, R., Moyzis, R. K., Bradbury, E. M., and Gupta, G. (1996) Solution structures of the individual single strands of the fragile X DNA triplets (GCC)n.(GGC)n, *Nucleic Acids Res. 24*, 784−792.
20. Petruska, J., Arnheim, N., and Goodman, M. F. (1996) Stability of intrastrand hairpin structures formed by the CAG/CTG class of DNA triplet repeats associated with neurological diseases, *Nucleic Acids Res. 24*, 1992−1998.
21. Petruska, J., Hartenstine, M. J., and Goodman, M. F. (1998) Analysis of strand slippage in DNA polymerase expansions of CAG/CTG triplet repeats associated with neurodegenerative disease, *J. Biol. Chem. 273*, 5204−5210.
22. Fry, M., and Loeb, L. A. (1994) The fragile X syndrome $d(CGG)_n$ nucleotide repeats form a stable tetrahelical structure, *Proc. Natl. Acad. Sci. U.S.A. 91*, 4950−4954.
23. Amrane, S., Sacca, B., Mills, M., Chauhan, M., Klump, H. H., and Mergny, J.-L. (2005) Length-dependent energetics of (CTG)n and (CAG)n trinucleotide repeats, *Nucleic Acids Res. 33*, 4065−4077.
24. Paiva, A. M., and Sheardy, R. D. (2005) The influence of sequence context and length on the kinetics of DNA duplex formation from complementary hairpins possessing (CNG) repeats, *J. Am. Chem. Soc. 127*, 5581−5585.
25. Paiva, A. M., and Sheardy, R. D. (2004) Influence of sequence context and length on the structure and stability of triplet repeat DNA oligomers, *Biochemistry 43*, 14218−14227.
26. Völker, J., Klump, H. H., and Breslauer, K. J. (2007) DNA metastability and biological regulation: conformational dynamics of metastable Ω-DNA bulge loops, *J. Am. Chem. Soc. 129*, 5272−5280.
27. Patel, N., Berglund, H., Nilsson, L., Rigler, R., McLaughlin, L. W., and Graslund, A. (1992) Thermodynamics of interaction of a fluorescent DNA oligomer with the anti-tumour drug netropsin, *Eur. J. Biochem. 203*, 361−366.
28. Law, S. M., Eritja, R., Goodman, M. F., and Breslauer, K. J. (1996) Spectroscopic and calorimetric characterizations of DNA duplexes containing 2-aminopurine, *Biochemistry 35*, 12329−12337.
29. Sowers, L. C., Boulard, Y., and Fazakerley, G. V. (2000) Multiple structures for the 2-aminopurine-cytosine mispair, *Biochemistry 39*, 7613−7620.
30. Sowers, L. C., Fazakerley, G. V., Eritja, R., Kaplan, B. E., and Goodman, M. F. (1986) Base pairing and mutagenesis: observation of a protonated base pair between 2-aminopurine and cytosine in an oligonucleotide by proton NMR, *Proc. Natl. Acad. Sci. U.S.A. 83*, 5434−5438.
31. Fagan, P. A., Fabrega, C., Eritja, R., Goodman, M. F., and Wemmer, D. E. (1996) NMR study of the conformation of the 2-aminopurine:cytosine mismatch in DNA, *Biochemistry 35*, 4026−4033.
32. Jean, J. M., and Hall, K. B. (2004) Stacking-unstacking dynamics of oligodeoxynucleotide trimers, *Biochemistry 43*, 10277−10284.
33. Jean, J. M., and Hall, K. B. (2002) 2-Aminopurine electronic structure and fluorescence properties in DNA, *Biochemistry 41*, 13152−13161.
34. Jean, J. M., and Hall, K. B. (2001) 2-Aminopurine fluorescence quenching and lifetimes: role of base stacking, *Proc. Natl. Acad. Sci. U.S.A. 98*, 37−41.
35. Somsen, O. J., Keukens, L. B., de Keijzer, M. N., van Hoek, A., and van Amerongen, H. (2005) Structural heterogeneity in DNA:

temperature dependence of 2-aminopurine fluorescence in dinucleotides, *ChemPhysChem 6*, 1622−1627.
36. Davis, S. P., Matsumura, M., Williams, A., and Nordlund, T. M. (2003) Position dependence of 2-aminopurine spectra in adenosine pentadeoxynucleotides, *J. Fluoresc. 13*, 249−259.
37. Kawai, M., Lee, M. J., Evans, K. O., and Nordlund, T. M. (2001) Temperature and base sequence dependence of 2-aminopurine fluorescence bands in single- and double-stranded oligodeoxynucleotides, *J. Fluoresc. 11*, 23−32.
38. Gargallo, R., Vives, M., Tauler, R., and Eritja, R. (2001) Protonation studies and multivariate curve resolution on oligodeoxynucleotides carrying the mutagenic base 2-aminopurine, *Biophys. J. 81*, 2886−2896.
39. O'Neill, M. A., and Barton, J. K. (2004) DNA-mediated charge transport requires conformational motion of the DNA bases: elimination of charge transport in rigid glasses at 77 K, *J. Am. Chem. Soc. 126*, 13234−13235.
40. O'Neill, M. A., and Barton, J. K. (2002) 2-Aminopurine: a probe of structural dynamics and charge transfer in DNA and DNA: RNA hybrids, *J. Am. Chem. Soc. 124*, 13053−13066.
41. Fiebig, T., Wan, C., and Zewail, A. H. (2002) Femtosecond charge transfer dynamics of a modified DNA base: 2-aminopurine in complexes with nucleotides, *ChemPhysChem 3*, 781−788.
42. Wan, C., Fiebig, T., Schiemann, O., Barton, J. K., and Zewail, A. H. (2000) Femtosecond direct observation of charge transfer between bases in DNA, *Proc. Natl. Acad. Sci. U.S.A. 97*, 14052−14055.
43. Xu, D. G., and Nordlund, T. M. (2000) Sequence dependence of energy transfer in DNA oligonucleotides, *Biophys. J. 78*, 1042−1058.
44. Guest, C. R., Hochstrasser, R. A., Sowers, L. C., and Millar, D. P. (1991) Dynamics of mismatched base pairs in DNA, *Biochemistry 30*, 3271−3279.
45. Hochstrasser, R. A., Carver, T. E., Sowers, L. C., and Millar, D. P. (1994) Melting of a DNA helix terminus within the active site of a DNA polymerase, *Biochemistry 33*, 11971−11979.
46. Larsen, O. F., van Stokkum, I. H., Gobets, B., van Grondelle, R., and van Amerongen, H. (2001) Probing the structure and dynamics of a DNA hairpin by ultrafast quenching and fluorescence depolarization, *Biophys. J. 81*, 1115−1126.
47. Lycksell, P. O., Graslund, A., Claesens, F., McLaughlin, L. W., Larsson, U., and Rigler, R. (1987) Base pair opening dynamics of a 2-aminopurine substituted Eco RI restriction sequence and its unsubstituted counterpart in oligonucleotides, *Nucleic Acids Res. 15*, 9011−9025.
48. Nordlund, T. M., Andersson, S., Nilsson, L., Rigler, R., Graslund, A., and McLaughlin, L. W. (1989) Structure and dynamics of a fluorescent DNA oligomer containing the EcoRI recognition sequence: fluorescence, molecular dynamics, and NMR studies, *Biochemistry 28*, 9095−9103.
49. Rachofsky, E. L., Osman, R., and Ross, J. B. (2001) Probing structure and dynamics of DNA with 2-aminopurine: effects of local environment on fluorescence, *Biochemistry 40*, 946−956.
50. Sarzynska, J., and Kulinski, T. (2005) Dynamics and stability of GCAA tetraloops with 2-aminopurine and purine substitutions, *J. Biomol. Struct. Dyn. 22*, 425−439.
51. Stivers, J. T. (1998) 2-Aminopurine fluorescence studies of base stacking interactions at abasic sites in DNA: metal-ion and base sequence effects, *Nucleic Acids Res. 26*, 3837−3844.
52. Xu, D., Evans, K. O., and Nordlund, T. M. (1994) Melting and premelting transitions of an oligomer measured by DNA base fluorescence and absorption, *Biochemistry 33*, 9592−9599.
53. Shafirovich, V., Dourandin, A., Huang, W., Luneva, N. P., and Geacintov, N. E. (1999) Oxidation of guanine at a distance in oligonucleotides induced by two-photon photoionization of 2-aminopurine, *J. Phys. Chem. B 103*, 10924−10933.
54. Shafirovich, V., Dourandin, A., Huang, W., Luneva, N. P., and Geacintov, N. E. (2000) Electron transfere at a distance induced by site selective photoionization of 2-aminopurine in oligonucleotides and investigated by transient absorption techniques, *Phys. Chem. Chem. Phys. 2*, 4399−4408.
55. Snell, F. D., and Snell, C. T. (1972) Colorimetric methods of analysis, including some turbidimetric and nephelometric methods, R. E. Krieger Pub. Co., Huntington, NY.
56. Plum, G. E. (2000) Optical Methods, in *Current Protocols in Nucleic Acid Chemistry*, Vol. 2, pp 7.3.1−7.3.17, John Wiley & Sons, Inc., New York, NY.
57. Breslauer, K. J. (1995) Extracting thermodynamic data from equilibrium melting curves for oligonucleotide order-disorder transitions, *Methods Enzymol. 259*, 221−242.
58. Breslauer, K. J. (1994) Protocols for oligonucleotide conjugates: synthesis and analytical techniques, in *Methods in Molecular Biology* (Agrawal, S., Ed.) Vol. 26, pp 347−372, Humana Press, Totowa, NJ.
59. Marky, L. A., and Breslauer, K. J. (1987) Calculating thermodynamic data for transitions of any molecularity from equilibrium melting curves, *Biopolymers 26*, 1601−1620.
60. Cantor, C. R., and Schimmel, P. R. (1980) Techniques for the study of biological structure and function, W. H. Freeman, San Francisco, CA.
61. Grant, C. D., DeRitter, M. R., Steege, K. E., Fadeeva, T. A., and Castner, E. W., Jr. (2005) Fluorescence probing of interior, interfacial, and exterior regions in solution aggregates of poly(ethylene oxide)-poly(propylene oxide)-poly(ethylene oxide) triblock copolymers, *Langmuir 21*, 1745−1752.
62. Sun, Y., Castner, E. W., Jr., Lawson, C. L., and Falkowski, P. G. (2004) Biophysical characterization of natural and mutant fluorescent proteins cloned from zooxanthellate corals, *FEBS Lett. 570*, 175−183.
63. Cross, A. J., and Fleming, G. R. (1984) Analysis of time-resolved fluorescence anisotropy decays, *Biophys. J. 46*, 45−56.
64. Hall, K. B., and Williams, D. J. (2004) Dynamics of the IRE RNA hairpin loop probed by 2-aminopurine fluorescence and stochastic dynamics simulations, *RNA 10*, 34−47.
65. Zagorowska, I., and Adamiak, R. W. (1996) 2-Aminopurine labelled RNA bulge loops. Synthesis and thermodynamics, *Biochimie 78*, 123−130.
66. Kaul, M., Barbieri, C. M., and Pilch, D. S. (2004) Fluorescence-based approach for detecting and characterizing antibiotic-induced conformational changes in ribosomal RNA: comparing aminoglycoside binding to prokaryotic and eukaryotic ribosomal RNA sequences, *J. Am. Chem. Soc. 126*, 3447−3453.
67. Menger, M., Eckstein, F., and Porschke, D. (2000) Dynamics of the RNA hairpin GNRA tetraloop, *Biochemistry 39*, 4500−4507.
68. Johnson, N. P., Baase, W. A., and Von Hippel, P. H. (2004) Low-energy circular dichroism of 2-aminopurine dinucleotide as a probe of local conformation of DNA and RNA, *Proc. Natl. Acad. Sci. U.S.A. 101*, 3426−3431.
69. Nordlund, T. M., Xu, D., and Evans, K. O. (1993) Excitation energy transfer in DNA: duplex melting and transfer from normal bases to 2-aminopurine, *Biochemistry 32*, 12090−12095.
70. Jean, J. M., and Krueger, B. P. (2006) Structural fluctuations and excitation transfer between adenine and 2-aminopurine in single-stranded deoxytrinucleotides, *J. Phys. Chem. B 110*, 2899−2909.
71. O'Neill, M. A., Becker, H. C., Wan, C., Barton, J. K., and Zewail, A. H. (2003) Ultrafast dynamics in DNA-mediated electron transfer: base gating and the role of temperature, *Angew. Chem., Int. Ed. 42*, 5896−5900.
72. Lipari, G., and Szabo, A. (1980) Effect of librational motion on fluorescence depolarization and nuclear magnetic resonance relaxation in macromolecules and membranes, *Biophys. J. 30*, 489−506.
73. Kinosita, K., Jr., Kawato, S., and Ikegami, A. (1977) A theory of fluorescence polarization decay in membranes, *Biophys. J. 20*, 289−305.
74. Valeur, B. (2002) Molecular fluorescence: principles and applications, Wiley-VCH, Weinheim, New York.
75. Lakowicz, J. R. (1999) Principles of fluorescence spectroscopy, 2nd ed., Kluwer Academic/Plenum, New York.
76. Millar, D. P. (1996) Fluorescence studies of DNA and RNA structure and dynamics, *Curr. Opin. Struct. Biol. 6*, 322−326.
77. Rai, P., Cole, T. D., Thompson, E., Millar, D. P., and Linn, S. (2003) Steady-state and time-resolved fluorescence studies indicate an unusual conformation of 2-aminopurine within ATAT and TATA duplex DNA sequences, *Nucleic Acids Res. 31*, 2323−2332.
78. Holmen, A., Norden, B., and Albinsson, B. (1997) Electronic transition moments of 2-aminopurine, *J. Am. Chem. Soc. 119*, 3114−3121.
79. Duhamel, J., Kanyo, J., Dinter-Gottlieb, G., and Lu, P. (1996) Fluorescence emission of ethidium bromide intercalated in defined DNA duplexes: evaluation of hydrodynamics components, *Biochemistry 35*, 16687−16697.

BI7005674